Research Square

Preprints are preliminary reports that have not undergone peer review.
They should not be considered conclusive, used to inform clinical practice,
or referenced by the media as validated information.

Improved model predictive control of permanent magnet synchronous motor based on lumped disturbance compensation

Liqun Huangfu
Huaiyin Institute of Technology
Chen Cen
Huaiyin Institute of Technology
Tao Zhang
zhangtaohyit@126.com

Huaiyin Institute of Technology

Research Article

Keywords: Permanent magnet synchronous motor, model predictive control, duty-cycle control, disturbance compensation

Posted Date: December 8th, 2023

DOI: https://doi.org/10.21203/rs.3.rs-3678797/v1

License: This work is licensed under a Creative Commons Attribution 4.0 International License.
Read Full License

Additional Declarations: No competing interests reported.

Improved model predictive control of permanent magnet synchronous motor based on lumped disturbance compensation

Liqun Huangfu, Chen Cen, Tao Zhang
Faculty of Electronic Information Engineering, Huaiyin Institute of Technology, Huaian, Jiangsu Province, China

Abstract: This paper proposes an improved finite control set model predictive current control (FCS-MPC) for permanent magnet synchronous motor (PMSM), including the use of a sliding mode observer for full electromagnetic parameter disturbance compensation and duty cycle control. First, a PMSM prediction model containing lumped disturbances was established. Second, a sliding mode observer is designed to estimate the lumped perturbation and compensate it to the reference voltage. The reference voltage is obtained based on the deadbeat principle and requires further constraints to obtain the optimal basic voltage vector. Then, a voltage-based cost function is constructed to calculate the duration of the non-zero optimal voltage vector and output the amplitude of the duty cycle adjustment voltage. Finally, experiments verify the effectiveness of the proposed FCS-MPC in improving robustness and steady-state performance.

Keywords: Permanent magnet synchronous motor; model predictive control; duty-cycle control; disturbance compensation

1. Introduction

In recent years, with the excessive use of fossil energy, many countries and regions have been in a state of energy shortage. At the same time, traditional energy has caused huge damage to society and the living environment. Therefore, many countries, companies, and scholars have begun research on emerging energy sources. Wind power generation, new energy vehicles, etc. have become hot spots in research [1-4], in which motors play an important role. Currently, permanent magnet synchronous motors are widely researched and applied due to their advantages such as small size, high power density, and high efficiency [5-8].

High-performance motor control algorithms are very important for motor drive systems. Commonly used solutions in the industry are field-oriented control (FOC) [9-11] and direct torque control (DTC) [12-14]. FOC is limited by the internal current loop bandwidth and PI controller and is not suitable for occasions with high dynamic performance and robustness requirements. DTC uses Bang-Bang control to directly output switching actions based on torque and flux errors. Fast dynamic performance comes with high torque ripple and switching losses. At present, many modern control strategies have been studied, such as sliding mode variable structure control, adaptive control, internal model control, and model predictive control (MPC). Among them, model predictive control stands out because of its fast dynamic performance and its ability to handle systems with multiple input and output variable constraints in a unified and clear way [15-18].

MPC establishes a prediction model based on the system model, obtains the optimal voltage vector by minimizing the error between the reference value and the predicted value, and directly outputs the

switching action. According to whether the modulator is used, it can be divided into continuous control set MPC (CCS-MPC) and finite control set MPC (FCS-MPC) [19-22]. FCS-MPC is more intuitive and simple and has a faster dynamic response. The principle of finite control sets is even extended to sensorless applications, where the discrete position angles are substituted into the cost function based on the back electromotive force as a spare set to obtain the optimal value [23-26]. MPC's vector selection is more accurate than DTC's. Although FCS-MPC has a faster dynamic response than FOC, its steady-state performance is slightly worse because one control cycle only outputs a voltage vector with fixed phase and amplitude. To solve this problem, many schemes have been proposed, such as virtual vector scheme, duty cycle control, and multi-vector strategy [27-30]. In [31], a combination of a non-zero vector and a zero vector is output in one control period by calculating the duration of the non-zero vector. In [32], a virtual vector is constructed on the basis of the inherent basic vector of the inverter to adjust the output voltage phase. However, the introduction of virtual vectors will exponentially increase the computational burden. Furthermore, a generalized double-vector predictive control based on the synthesis of two non-zero vectors is proposed in [33]. In [34], it is further expanded to add a zero vector to realize three-vector predictive control. However, the above scheme introduces a modulator, and MPC loses its fast dynamic performance.

Furthermore, another factor affecting prediction accuracy is parameter dependence. The prediction model established by FCS-MPC for PMSM based on the system model will no longer be accurate when subject to external interference or internal temperature rise, further deteriorating the control performance [35-38]. Commonly used robust schemes can be divided into prediction model improvement, parameter identification, and observer-based estimation compensation schemes [39]. Predictive model improvement solutions such as driver solutions require a large amount of data training and have high data quality requirements [40-43]. Parameter identification often requires the identification of multiple parameters, which increases the complexity of the system [44-46]. Therefore, the observer-based estimation compensation scheme (OBEC) has gained more favor. OBEC uniformly estimates and compensates for the lumped disturbance caused by parameter mismatch, making it simpler and easier to understand [47-50]. A composite sliding mode controller is proposed in [51] to estimate the error and use it as a voltage compensation to the reference voltage of the deadbeat predictive control (DPCC) output. In [52], a robust control scheme combining DPCC with stator current and disturbance observer is proposed, which also achieves the same effect. However, the compensation voltage obtained by this type of estimation is more suitable for non-finite set model predictive control.

This paper proposes a finite set predictive current robust control scheme that combines duty cycle model predictive control and observation compensation. A voltage positioning scheme based on the deadbeat principle is used to determine the reference voltage and the reference voltage is constrained to obtain the optimal basic voltage vector, thus reducing the computational burden caused by iterative calculations. On this basis, the sliding mode observer is used to estimate the lumped disturbance and compensate for the reference voltage, which reduces the parameter sensitivity of the system. The remainder of this article is organized as follows. Section 2 describes and analyzes the modeling of PMSM and traditional FCS-MPC. Section 3 presents the design of the machine model and sliding mode observer incorporating lumped perturbations. Then, in Section 4, the overall implementation of duty

cycle control with SMO is described. The experimental results are shown in Section 5, and the conclusions are shown in Section 6.

2. The modeling of PMSM and FCS-MPC

2.1. Mathematical modeling

Since the surface-mounted permanent magnet synchronous motor (SPMSM) satisfies L_d=L_q=L, the voltage equation of the SPMSM established in the rotating coordinate system is as follows:

$$\begin{cases} U_d = R_s i_d + L\dfrac{di_d}{dt} - \omega L i_q \\ U_q = R_s i_q + L\dfrac{di_q}{dt} + \omega L i_d + \omega \psi_f \end{cases} \tag{1}$$

where U, i, and ω are the stator voltage, stator current, and electrical angular velocity, respectively. R_s, ψ_f, and L represent stator resistance, flux linkage, and inductance.

The electromagnetic torque equation of the SPMSM is given by

$$T_e = \frac{3}{2} P i_q \psi_f \tag{2}$$

where P is the number of pole pairs of SPMSM.

2.2. Finite control set model predictive control

FCS-MPC uses the Euler formula to discretize the PMSM model, uses the current as the control variable, and takes one step forward to obtain the predicted value of the future moment:

$$\begin{cases} i_d^{\,k+1} = (1 - \dfrac{R_s T_s}{L}) i_d^{\,k} + \dfrac{T_s}{L} U_d(i) + T_s \omega i_q^{\,k} \\ i_q^{\,k+1} = (1 - \dfrac{R_s T_s}{L}) i_q^{\,k} + \dfrac{T_s}{L} U_q(i) - T_s \omega i_d^{\,k} - \dfrac{T_s \psi_f \omega}{L} \end{cases} \tag{3}$$

where T_s is the control time, $U(i)$ represents the voltage component generated by the inherent basic voltage vector of the inverter, k and k+1 represent the current moment and the next moment, respectively.

The optimal voltage vector is selected by minimizing the cost function of the current tracking error. This article uses the two-level voltage source inverter. The cost function of MPCC is defined as follows:

$$J = (i_{dq}^{ref} - i_{dq}^{\,k+1})^2 \tag{4}$$

where i_{dq}^{ref} represents the reference current.

The block diagram of conventional FCS-MPC is shown in Figure 1.

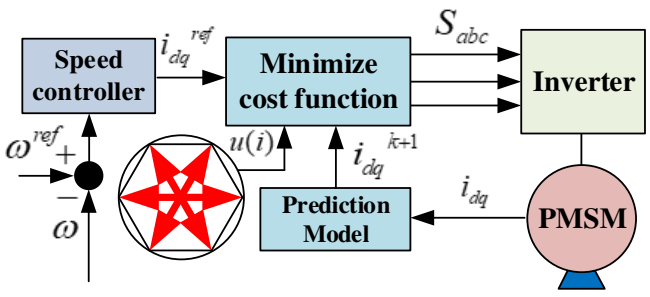


Figure 1. Block diagram of conventional FCS-MPC.

3. Lumped disturbance model and sliding mode observer design

Taking into account all electromagnetic parameter mismatches produces lumped perturbations and rewrites the voltage equation:

$$\begin{cases} U_d = R_s i_d + L\dfrac{di_d}{dt} - \omega L i_q + \varepsilon_d \\ \varepsilon_d = \Delta R_s i_d + \Delta L\dfrac{di_d}{dt} - \omega \Delta L i_q \\ \dfrac{d\varepsilon_d}{dt} = \delta_d \end{cases} \tag{5}$$

$$\begin{cases} U_q = R_s i_q + L\dfrac{di_q}{dt} + \omega L i_d + \omega \psi_f + \varepsilon_q \\ \varepsilon_q = \Delta R_s i_q + \Delta L\dfrac{di_q}{dt} + \omega \Delta L i_d + \omega \Delta \psi_f \\ \dfrac{d\varepsilon_q}{dt} = \delta_q \end{cases} \tag{6}$$

where ε_{dq} are electromagnetic parameter disturbances.

Based on (3), the lumped disturbance design observer is estimated as follows

$$\begin{cases} U_d = R_s \hat{i}_d + L\dfrac{d\hat{i}_d}{dt} - \omega L \hat{i}_q + \hat{\varepsilon}_d + F_d \\ U_q = R_s \hat{i}_q + L\dfrac{d\hat{i}_q}{dt} + \omega L \hat{i}_d + \omega \psi_f + \hat{\varepsilon}_q + F_q \\ \dfrac{d\hat{\varepsilon}_d}{dt} = c_d F_d \\ \dfrac{d\hat{\varepsilon}_q}{dt} = c_q F_q \end{cases} \tag{7}$$

where F and c are sliding mode control function and sliding mode parameters, respectively, $\hat{i}$ and $\hat{\varepsilon}$ represent the estimated current and electromagnetic parameter disturbances.

Combining (5)-(7), the error between the actual value and the observed value is:

$$\begin{cases} \dfrac{de_1}{dt} = -\dfrac{1}{L}(Re_1 + e_3 + F_d) \\ \dfrac{de_2}{dt} = -\dfrac{1}{L}(Re_2 + e_4 + F_q) \\ \dfrac{de_3}{dt} = c_d F_d - \delta_d \\ \dfrac{de_4}{dt} = c_q F_q - \delta_q \end{cases} \tag{8}$$

where $e_1 = \hat{i}_d - i_d$, $e_2 = \hat{i}_q - i_q$, $e_3 = \hat{\varepsilon}_d - \varepsilon_d$ and $e_4 = \hat{\varepsilon}_q - \varepsilon_q$.

A sliding mode observer is used to converge the error, and a simple linear sliding mode surface is selected:

$$s_d = \hat{i}_d - i_d, s_q = \hat{i}_q - i_q \tag{9}$$

To improve the observation accuracy and convergence speed of the sliding mode observer, a power term is added based on the exponential approaching law to design the sliding mode control function:

$$\frac{ds}{dt} = -k_1 \operatorname{sgn}(s) - \lambda s|s|^{\alpha} \tag{10}$$

where, λ>0, k_1>0 and 0<α<1.

Substituting (9) into (10) yields

$$\begin{cases} \dfrac{d}{dt}e_1 = -\lambda e_1 |e_1|^{\alpha} - k_1 \operatorname{sgn}(e_1) \\ \dfrac{d}{dt}e_2 = -\lambda e_2 |e_2|^{\alpha} - k_1 \operatorname{sgn}(e_2) \end{cases} \tag{11}$$

Treat e_3 and e_4 as disturbances of the control function and ignore them. Combined with (8) and (11), design the following sliding mode control function:

$$\begin{cases} F_d = L[\lambda e_1 |e_1|^{\alpha} + k_1 \operatorname{sgn}(e_1)] - R_s e_1 \\ F_q = L[\lambda e_2 |e_2|^{\alpha} + k_1 \operatorname{sgn}(e_2)] - R_s e_2 \end{cases} \tag{12}$$

In addition, to make the estimated stator current and lumped disturbance converge, the parameters of the observer need to be designed according to the Lyapunov function:

$$V = \frac{1}{2}s^2, \frac{dV}{dt} = s \cdot \frac{ds}{dt} \le 0 \tag{13}$$

Taking the d-axis as an example, substitute the error term into (13). Combined with (7), (8) and (10), the stability condition is rewritten as follows:

$$\frac{dV_d}{dt} = -\frac{1}{L}e_1 e_3 - \lambda e_1^{\,2} |e_1|^{\alpha} - k_1 e_1 \operatorname{sgn}(e_1) \le 0 \tag{14}$$

Under the condition of stability, the parameters k_1 in the d-q axis were obtained.

$$k_1 \ge \frac{1}{L}\max(|e_3|, |e_4|) \tag{15}$$

The above analysis proves that SMO is stable with appropriate parameters.

4. Duty-cycle FCS-MPC based on SMO

After obtaining (12), the voltage equation of the observer is discretized.

$$\begin{cases} \hat{i}_d^{\,k+1} = (1 - \dfrac{R_s T_s}{L})\hat{i}_d^{\,k} + \dfrac{T_s}{L}U_d + T_s \omega i_q^{\,k} - \dfrac{T_s}{L}\hat{\varepsilon}_d^{\,k} - \dfrac{T_s}{L}F_d \\ \hat{i}_q^{\,k+1} = (1 - \dfrac{R_s T_s}{L})\hat{i}_q^{\,k} + \dfrac{T_s}{L}U_q - T_s \omega i_d^{\,k} - \dfrac{T_s \psi_f}{L}\omega - \dfrac{T_s}{L}\hat{\varepsilon}_q^{\,k} - \dfrac{T_s}{L}F_q \\ \hat{\varepsilon}_d^{\,k+1} = c_d T_s F_d + \hat{\varepsilon}_d \\ \hat{\varepsilon}_q^{\,k+1} = c_q T_s F_q + \hat{\varepsilon}_q \end{cases} \tag{16}$$

Traditional model predictive control requires 8 iterations to calculate the optimal voltage vector. To reduce the computational burden, the optimal voltage vector is obtained by referring to the deadbeat principle.

$$\begin{cases} U_d^{\,\mathrm{ref}} = \dfrac{L}{T_s}[i_d^{ref} - (1 - \dfrac{R_s T_s}{L})\hat{i}_d^{\,k+1} - T_s \omega \hat{i}_q^{\,k+1}] \\ U_q^{\,\mathrm{ref}} = \dfrac{L}{T_s}[i_q^{ref} - (1 - \dfrac{R_s T_s}{L})\hat{i}_q^{\,k+1} + T_s \omega \hat{i}_d^{\,k+1} + \dfrac{T_s \psi_f \omega}{L}] \end{cases} \tag{17}$$

The above-mentioned reference voltage obtained is an unconstrained solution because FCS-MPC needs to obtain the optimal value from the inherent 8 voltage vectors [53], so next it is necessary to locate the optimal voltage vector based on the reference voltage. The method is to calculate the angle of the reference voltage in the stationary coordinate system α-β to determine the optimal value as

shown in figure 2. This solution reduces eight calculations to one, significantly reducing the computational burden.

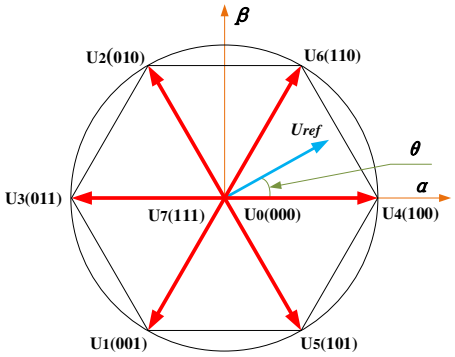


Figure 2. Voltage positioning method based on deadbeat principle.

To improve the accuracy of voltage output, duty cycle control is introduced to adjust the output amplitude. According to (17), the cost function is rewritten in the form of voltage:

$$J_1 = (U^{ref} - \frac{U_{opt} t_{opt}}{T_S})^2 \tag{18}$$

where U_{opt} and t_{opt} are the optimal voltage vector and its duration.

Taking the partial derivative of the duration in the cost function obtains the corresponding duration and limits it between 0 and T_s.

$$t_{opt} = \frac{U^{ref} \bullet U_{opt}}{\left|U_{opt}\right|^2} T_S \tag{19}$$

When the duration of the non-zero optimal vector is calculated, the zero vector adjustment amplitude will be output for the remaining time, thereby improving the steady-state performance of the system.

The overall proposed FCS-MPC is shown in Figure 3.

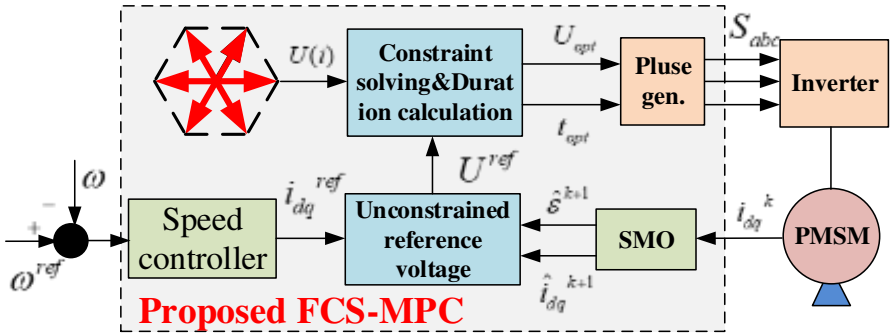


Figure 3. Block diagram of the proposed FCS-MPC.

5. Experimental result

Figure 4 shows the construction of the experimental device, and the relevant SPMSM parameters are shown in Table 1. To verify the improvement of robust performance and steady-state performance of the proposed scheme, it is compared with traditional FCS-MPC.



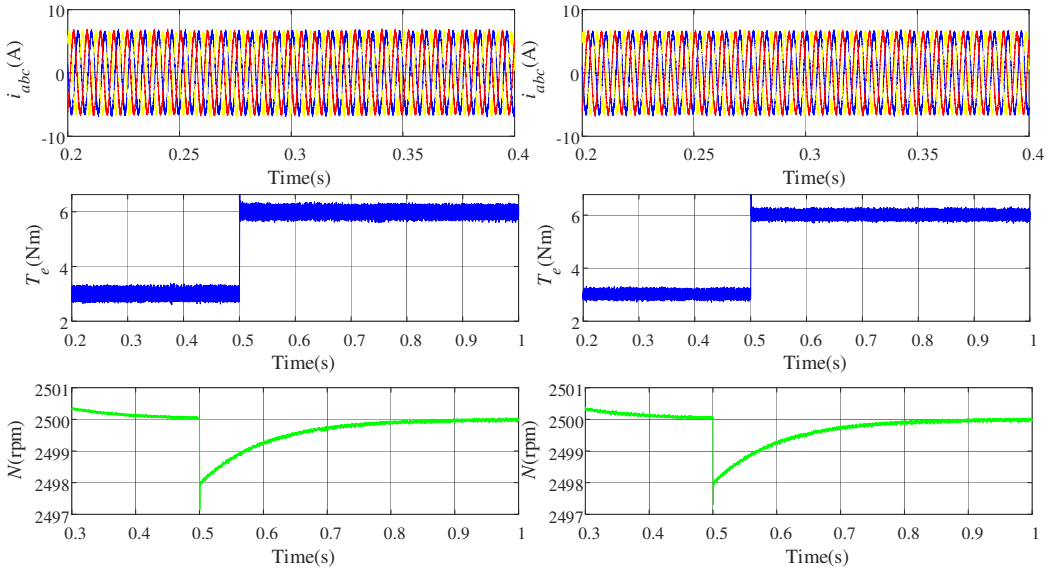
Figure 4. The experiment platform.

Table 1. SPMSM system parameters.

Parameters	values
Inductance	6.6 mH
Resistance	1.6 Ω
Number of pole pairs	4
Rated speed	2500 rpm
Rated power	3.8 kW
Rated torque	15 Nm
Inertia	0.00277 kg.m^2

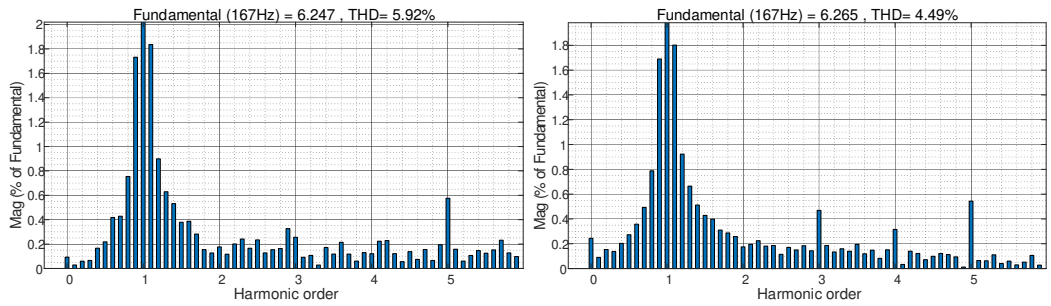
5.1. Comparison of steady-state performance

To verify that the introduced duty cycle control improves the steady-state performance of FCS-MPC, we compared the proposed scheme under normal parameters with the traditional single voltage vector output FCS-MPC.



(a) (b)

Figure 5. Comparison of three-phase current, torque, and speed under normal parameters. (a) Conventional FCS-MPC, (b) the proposed FCS-MPC.



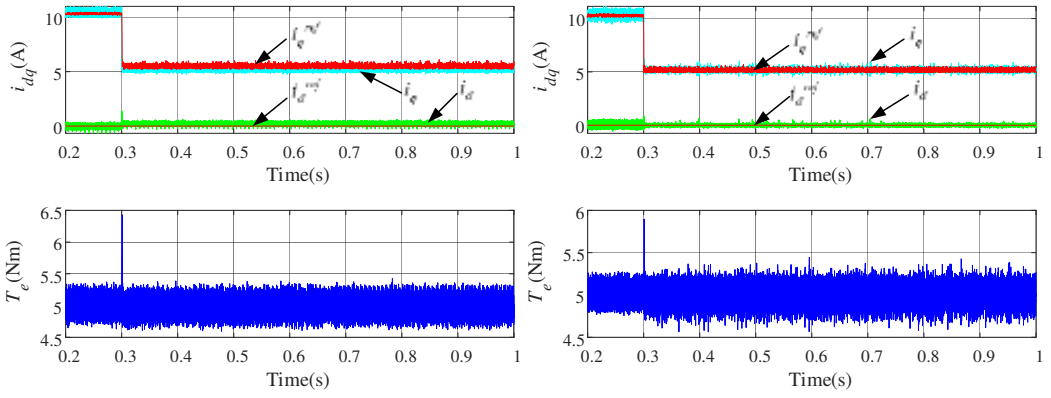
(a) (b)

Figure 6. Comparison of THD of stator current under normal parameters. (a) Conventional FCS-MPC, (b) the proposed FCS-MPC.

Figure 5 shows the comparison of torque and three-phase current between the two schemes when the load changes from 3Nm to 6Nm at 2500rpm. To further illustrate the improvement of steady-state performance, Figure 6 shows the THD comparison of the stator current of the two schemes.

It can be observed from figure 5 that the two schemes have similar dynamic performance, and the steady-state performance of the proposed scheme is further improved due to the use of zero vectors. The torque ripple in Figure 5 is expressed in standard deviation as 1.4587 Nm and 1.3963 Nm respectively. The harmonics of the traditional scheme and the proposed scheme are 5.92% and 4.49% respectively in Figure 6. Therefore, it can be concluded that the introduction of the duty cycle makes the voltage selection more accurate, resulting in a smaller tracking error of FCS-MPC, and the corresponding steady-state performance is improved.

5.2. Comparison of robust performance



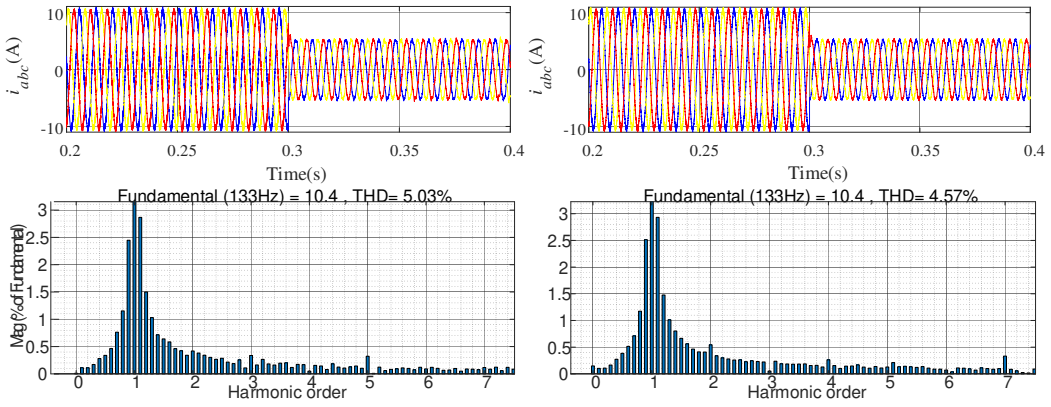
(a) (b)

Figure 7. Comparison of current tracking, torque under R_s=3R_{s0}, ψ_f=2$\psi_{f0,}$ and L=2L_0. (a) Conventional FCS-MPC, (b) Proposed FCS-MPC.

Since the motor cannot change parameters at will, robustness verification is achieved by changing the parameters of the motor in the control program. Figures 7 and 8 respectively show the waveform comparison between the traditional scheme and the proposed scheme under all electromagnetic parameter adaptations. The working speed of the motor is 2000rpm. The electromagnetic parameters in the controller are set to mutate at t=0.3s.

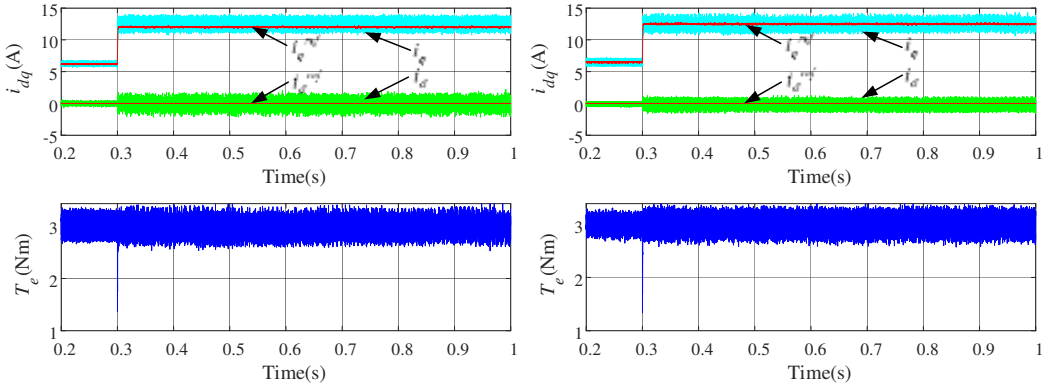
Figure 7 shows the *d*-*q* current tracking error under R_s=3R_{s0}, ψ_f=2$\psi_{f0,}$ and L=2L_0. R_{s0}, $\varphi_{f0,}$ and L_0 represent the nominal values of the motor. It can be seen that the current tracking of the traditional

FCS-MPC is offset under parameter changes. The *d*-axis and *q*-axis deviation are 0.1487A and 0.2887a, and the *d*-axis and *q*-axis deviation after SMO compensation are 0.0951A and 0.0895A. The torque ripples are 1.4587 Nm and 1.3724 Nm respectively. Figure 8 shows that the harmonics of the phase current are reduced from 5.03% to 4.57% after using SMO to compensate for the lumped disturbance.



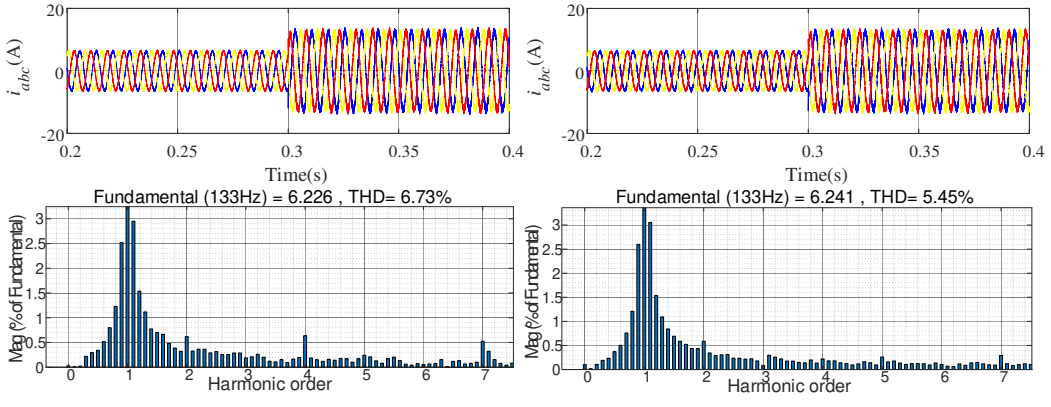
(a) (b)

Figure 8. Comparison of current harmonics under R_s=3R_{s0}, ψ_f=2$\psi_{f0,}$ and L=2L_0. (a) Conventional FCS-MPC, (b) Proposed FCS-MPC.



(a) (b)

Figure 9. Comparison of current tracking, torque under R_s=0.5R_{s0}, ψ_f=0.5$\psi_{f0,}$ and L=0.5L_0. (a) Conventional FCS-MPC, (b) Proposed FCS-MPC.



(a) (b)

Figure 10. Comparison of current harmonics under R_s=0.5R_{s0}, ψ_f=0.5$\psi_{f0,}$ and L=0.5L_0. (a) Conventional FCS-MPC, (b) Proposed FCS-MPC.

Similarly, Figure 9 shows the *d*-*q* current tracking error under R_s=0.5R_{s0}, ψ_f=0.5$\psi_{f0,}$ and L=0.5L_0. The *d*-axis and *q*-axis current tracking deviation of the traditional FCS-MPC are 0.1278A and 0.1898A,

while the deviation after SMO compensation is 0. 1019A and 0.1362A. The torque ripples of the two schemes are 1.456Nm and 1.426Nm respectively. Figure 10 shows that the harmonics of the phase current are reduced from 6.73% to 5.45% after SMO compensation.

Through the above analysis, it can be known that the proposed sliding mode observer can effectively reduce the sensitivity of parameters by estimating the lumped disturbance and performing voltage compensation. Overall, the proposed scheme is improved compared to traditional FCS-MPC in terms of steady-state performance and robust performance.

6. Conclusion

This paper proposes a lumped disturbance compensation duty cycle FCS-MPC, which combines a sliding mode observer and duty cycle FCS-MPC. In this study, a sliding mode observer is used to estimate the lumped perturbation caused by the electromagnetic parameter band mismatch and is used to compensate for the reference voltage, which reduces the parameter sensitivity of the current loop. In addition, the reference voltage is obtained using the deadbeat principle. The unconstrained reference voltage obtained at this time needs to be further positioned in the vector space to calculate the inherent optimal voltage vector of the inverter. This scheme only needs to be calculated once, which greatly reduces the computational burden. The effectiveness of the proposed FCS-MPC is verified by comparing experimental results. Compared with traditional FCS-MPC, the proposed control scheme can improve steady-state performance and system robustness while maintaining fast dynamic performance.

Ethical Approval: This article does not involve ethics; therefore ethical approval is not required. All authors consent to publish.

Fundings: This research was funded by Jiangsu Province Higher Education Basic Science (Natural Science) Research Major Project, grant number 23KJA470001" and funded by Huaian City Key R&D Plan Projects, grant number HAG202302.

Data Availability Statement: Availability of data and materials: Data are contained within the article.

References

1. Sun, X.; Shi, Z.; Cai, Y.; Lei, G.; Guo, Y.; Zhu, J. Driving-Cycle-Oriented Design Optimization of a Permanent Magnet Hub Motor Drive System for a Four-Wheel-Drive Electric Vehicle. *IEEE Transactions on Transportation Electrification* **2020**, *6*, 1115-1125, doi:10.1109/TTE.2020.3009396.
2. Priyadarshi, N.; Bhaskar, M.S.; Almakhles, D. A Novel Hybrid Whale Optimization Algorithm Differential Evolution Algorithm-Based Maximum Power Point Tracking Employed Wind Energy Conversion Systems for Water Pumping Applications: Practical Realization. *IEEE Transactions on Industrial Electronics* **2024**, *71*, 1641-1652, doi:10.1109/TIE.2023.3260345.
3. Sun, X.; Hu, C.; Zhu, J.; Wang, S.; Zhou, W.; Yang, Z.; Lei, G.; Li, K.; Zhu, B.; Guo, Y. MPTC for PMSMs of EVs With Multi-Motor Driven System Considering Optimal Energy Allocation. *IEEE Transactions on Magnetics* **2019**, *55*, 1-6, doi:10.1109/TMAG.2019.2904289.
4. Chen, L.; Xu, H.; Sun, X. A Novel Strategy of Control Performance Improvement for Six-Phase Permanent Magnet Synchronous Hub Motor Drives of EVs Under New European Driving Cycle. *IEEE Transactions on Vehicular Technology* **2021**, *70*, 5628-5637, doi:10.1109/TVT.2021.3079576.

5. Sun, X.; Zhang, Y.; Tian, X.; Cao, J.; Zhu, J. Speed Sensorless Control for IPMSMs Using a Modified MRAS With Gray Wolf Optimization Algorithm. *IEEE Transactions on Transportation Electrification* **2022**, *8*, 1326-1337, doi:10.1109/TTE.2021.3093580.
6. Fu, R. Robust Model Predictive Flux Control of PMSM Drive Using a Compensated Stator Flux Predictor. *IEEE Access* **2021**, *9*, 136736-136743, doi:10.1109/ACCESS.2021.3117860.
7. Jin, Z.; Sun, X.; Lei, G.; Guo, Y.; Zhu, J. Sliding Mode Direct Torque Control of SPMSMs Based on a Hybrid Wolf Optimization Algorithm. *IEEE Transactions on Industrial Electronics* **2022**, *69*, 4534-4544, doi:10.1109/TIE.2021.3080220.
8. Bai, C.; Yin, Z.; Zhang, Y.; Liu, J. Multiple-Models Adaptive Disturbance Observer-Based Predictive Control for Linear Permanent-Magnet Synchronous Motor Vector Drive. *IEEE Transactions on Power Electronics* **2022**, *37*, 9596-9611, doi:10.1109/TPEL.2022.3155458.
9. Masiala, M.; Vafakhah, B.; Salmon, J.; Knight, A.M. Fuzzy Self-Tuning Speed Control of an Indirect Field-Oriented Control Induction Motor Drive. *IEEE Transactions on Industry Applications* **2008**, *44*, 1732-1740, doi:10.1109/TIA.2008.2006342.
10. Hannan, M.A.; Ali, J.A.; Mohamed, A.; Amirulddin, U.A.U.; Tan, N.M.L.; Uddin, M.N. Quantum-Behaved Lightning Search Algorithm to Improve Indirect Field-Oriented Fuzzy-PI Control for IM Drive. *IEEE Transactions on Industry Applications* **2018**, *54*, 3793-3805, doi:10.1109/TIA.2018.2821644.
11. Hadla, H.; Santos, F. Performance Comparison of Field-oriented Control, Direct Torque Control, and Model-predictive Control for SynRMs. *Chinese Journal of Electrical Engineering* **2022**, *8*, 24-37, doi:10.23919/CJEE.2022.000003.
12. Wang, X.; Wang, Z.; Xu, Z.; Cheng, M.; Hu, Y. Optimization of Torque Tracking Performance for Direct-Torque-Controlled PMSM Drives With Composite Torque Regulator. *IEEE Transactions on Industrial Electronics* **2020**, *67*, 10095-10108, doi:10.1109/TIE.2019.2962451.
13. Inoue, Y.; Morimoto, S.; Sanada, M. Comparative Study of PMSM Drive Systems Based on Current Control and Direct Torque Control in Flux-Weakening Control Region. *IEEE Transactions on Industry Applications* **2012**, *48*, 2382-2389, doi:10.1109/TIA.2012.2227134.
14. Choi, Y.S.; Choi, H.H.; Jung, J.W. Feedback Linearization Direct Torque Control With Reduced Torque and Flux Ripples for IPMSM Drives. *IEEE Transactions on Power Electronics* **2016**, *31*, 3728-3737, doi:10.1109/TPEL.2015.2460249.
15. Vazquez, S.; Rodriguez, J.; Rivera, M.; Franquelo, L.G.; Norambuena, M. Model Predictive Control for Power Converters and Drives: Advances and Trends. *IEEE Transactions on Industrial Electronics* **2017**, *64*, 935-947, doi:10.1109/TIE.2016.2625238.
16. Sun, X.; Wu, M.; Yin, C.; Wang, S. Model Predictive Thrust Force Control for Linear Motor Actuator used in Active Suspension. *IEEE Transactions on Energy Conversion* **2021**, *36*, 3063-3072, doi:10.1109/TEC.2021.3069843.
17. Elizondo, J.L.; Olloqui, A.; Rivera, M.; Macias, M.E.; Probst, O.; Micheloud, O.M.; Rodriguez, J. Model-Based Predictive Rotor Current Control for Grid Synchronization of a DFIG Driven by an Indirect Matrix Converter. *IEEE Journal of Emerging and Selected Topics in Power Electronics* **2014**, *2*, 715-726, doi:10.1109/JESTPE.2014.2349952.
18. Sun, X.; Wu, M.; Lei, G.; Guo, Y.; Zhu, J. An Improved Model Predictive Current Control for PMSM Drives Based on Current Track Circle. *IEEE Transactions on Industrial Electronics* **2021**, *68*, 3782-3793, doi:10.1109/TIE.2020.2984433.

19. Sun, X.; Su, Z.; Lei, G.; Cai, Y.; Yao, M. Adaptive Model-Free Predictive Current Control for SPMSM Drives with Optimal Virtual Vector Modulation. *IEEE/ASME Transactions on Mechatronics* accepted, doi: 10.1109/TMECH.2023.3332136.
20. Wang, F.; He, L.; Rodriguez, J. FPGA-Based Continuous Control Set Model Predictive Current Control for PMSM System Using Multistep Error Tracking Technique. *IEEE Transactions on Power Electronics* **2020**, *35*, 13455-13464, doi:10.1109/tpel.2020.2984336.
21. Sun, X.; Li, T.; Tian, X.; Zhu, J. Fault-Tolerant Operation of a Six-Phase Permanent Magnet Synchronous Hub Motor Based on Model Predictive Current Control With Virtual Voltage Vectors. *IEEE Transactions on Energy Conversion* **2022**, *37*, 337-346, doi:10.1109/TEC.2021.3109869.
22. Ahmed, A.A.; Koh, B.K.; Lee, Y.I. A Comparison of Finite Control Set and Continuous Control Set Model Predictive Control Schemes for Speed Control of Induction Motors. *IEEE Transactions on Industrial Informatics* **2018**, *14*, 1334-1346, doi:10.1109/TII.2017.2758393.
23. Sun, X.; Hu, C.; Lei, G.; Yang, Z.; Guo, Y.; Zhu, J. Speed Sensorless Control of SPMSM Drives for EVs With a Binary Search Algorithm-Based Phase-Locked Loop. *IEEE Transactions on Vehicular Technology* **2020**, *69*, 4968-4978, doi:10.1109/TVT.2020.2981422.
24. Abdelrahem, M.; Hackl, C.M.; Kennel, R. Finite Position Set-Phase Locked Loop for Sensorless Control of Direct-Driven Permanent-Magnet Synchronous Generators. *IEEE Transactions on Power Electronics* **2018**, *33*, 3097-3105, doi:10.1109/TPEL.2017.2705245.
25. Sun, X.; Cao, J.; Lei, G.; Guo, Y.; Zhu, J. Speed Sensorless Control for Permanent Magnet Synchronous Motors Based on Finite Position Set. *IEEE Transactions on Industrial Electronics* **2020**, *67*, 6089-6100, doi:10.1109/TIE.2019.2947875.
26. Sun, X.; Cai, F.; Yang, Z.; Tian, X. Finite Position Control of Interior Permanent Magnet Synchronous Motors at Low Speed. *IEEE Transactions on Power Electronics* **2022**, *37*, 7729-7738, doi:10.1109/TPEL.2022.3146841.
27. Xu, Y.; Ding, X.; Wang, J.; Li, Y. Three-vector-based low-complexity model predictive current control with reduced steady-state current error for permanent magnet synchronous motor. *IET Electric Power Applications* **2020**, *14*, 305-315, doi:10.1049/iet-epa.2019.0108.
28. Su, Z.; Sun, X.; Lei, G.; Yao, M. Model-Free Predictive Current Control for Dual Three-Phase PMSM Drives with An Optimal Modulation Pattern. *IEEE Transactions on Industrial Electronics* **accepted**, doi: 10.1109/TIE.2023.3327554.
29. Yan, Y.; Wang, S.; Xia, C.; Wang, H.; Shi, T. Hybrid Control Set-Model Predictive Control for Field-Oriented Control of VSI-PMSM. *IEEE Transactions on Energy Conversion* **2016**, *31*, 1622-1633, doi:10.1109/TEC.2016.2598154.
30. Wu, M.; Sun, X.; Zhu, J.; Lei, G.; Guo, Y. Improved Model Predictive Torque Control for PMSM Drives Based on Duty Cycle Optimization. *IEEE Transactions on Magnetics* **2021**, *57*, 1-5, doi:10.1109/TMAG.2020.3008495.
31. Sun, X.; Li, T.; Zhu, Z.; Lei, G.; Guo, Y.; Zhu, J. Speed Sensorless Model Predictive Current Control Based on Finite Position Set for PMSHM Drives. *IEEE Transactions on Transportation Electrification* **2021**, *7*, 2743-2752, doi:10.1109/TTE.2021.3081436.
32. Sun, X.; Li, T.; Yao, M.; Lei, G.; Guo, Y.; Zhu, J. Improved Finite-Control-Set Model Predictive Control With Virtual Vectors for PMSHM Drives. *IEEE Transactions on Energy Conversion* **2022**, *37*, 1885-1894, doi:10.1109/TEC.2021.3138905.

33. Zhang, Y.; Xu, D.; Huang, L. Generalized Multiple-Vector-Based Model Predictive Control for PMSM Drives. *IEEE Transactions on Industrial Electronics* **2018**, *65*, 9356-9366, doi:10.1109/TIE.2018.2813994.
34. Chen, L.; Xu, H.; Sun, X.; Cai, Y. Three-Vector-Based Model Predictive Torque Control for a Permanent Magnet Synchronous Motor of EVs. *IEEE Transactions on Transportation Electrification* **2021**, *7*, 1454-1465, doi:10.1109/TTE.2021.3053256.
35. Yang, J.; Chen, W.-H.; Li, S.; Guo, L.; Yan, Y. Disturbance/Uncertainty Estimation and Attenuation Techniques in PMSM Drives—A Survey. *IEEE Transactions on Industrial Electronics* **2017**, *64*, 3273-3285, doi:10.1109/TIE.2016.2583412.
36. Sun, X.; Zhang, Y.; Cai, Y.; Tian, X. Compensated Deadbeat Predictive Current Control Considering Disturbance and VSI Nonlinearity for In-Wheel PMSMs. *IEEE/ASME Transactions on Mechatronics* **2022**, *27*, 3536-3547, doi:10.1109/TMECH.2021.3135936.
37. Sun, X.; Cao, J.; Lei, G.; Guo, Y.; Zhu, J. A Composite Sliding Mode Control for SPMSM Drives Based on a New Hybrid Reaching Law With Disturbance Compensation. *IEEE Transactions on Transportation Electrification* **2021**, *7*, 1427-1436, doi:10.1109/TTE.2021.3052986.
38. Rodriguez, J.; Kazmierkowski, M.P.; Espinoza, J.R.; Zanchetta, P.; Abu-Rub, H.; Young, H.A.; Rojas, C.A. State of the Art of Finite Control Set Model Predictive Control in Power Electronics. *IEEE Transactions on Industrial Informatics* **2013**, *9*, 1003-1016, doi:10.1109/TII.2012.2221469.
39. Li, T.; Sun, X.; Lei, G.; Guo, Y.; Yang, Z.; Zhu, J. Finite-Control-Set Model Predictive Control of Permanent Magnet Synchronous Motor Drive Systems—An Overview. *IEEE/CAA Journal of Automatica Sinica* **2022**, *9*, 2087-2105, doi:10.1109/JAS.2022.105851.
40. Brosch, A.; Hanke, S.; Wallscheid, O.; Böcker, J. Data-Driven Recursive Least Squares Estimation for Model Predictive Current Control of Permanent Magnet Synchronous Motors. *IEEE Transactions on Power Electronics* **2021**, *36*, 2179-2190, doi:10.1109/TPEL.2020.3006779.
41. Wei, Y.; Young, H.; Wang, F.; Rodríguez, J. Generalized Data-Driven Model-Free Predictive Control for Electrical Drive Systems. *IEEE Transactions on Industrial Electronics* **2022**, 10.1109/TIE.2022.3210563, 1-11, doi:10.1109/TIE.2022.3210563.
42. Lin, C.; Liu, T.; Yu, J.; Fu, L.; Hsiao, C. Model-Free Predictive Current Control for Interior Permanent-Magnet Synchronous Motor Drives Based on Current Difference Detection Technique. *IEEE Transactions on Industrial Electronics* **2014**, *61*, 667-681, doi:10.1109/TIE.2013.2253065.
43. Carlet, P.G.; Favato, A.; Bolognani, S.; Dörfler, F. Data-Driven Continuous-Set Predictive Current Control for Synchronous Motor Drives. *IEEE Transactions on Power Electronics* **2022**, *37*, 6637-6646, doi:10.1109/TPEL.2022.3142244.
44. Chen, Z.; Qiu, J.; Jin, M. Adaptive finite-control-set model predictive current control for IPMSM drives with inductance variation. *IET Electric Power Applications* **2017**, *11*, 874-884, doi:10.1049/iet-epa.2016.0861.
45. Brosch, A.; Wallscheid, O.; Böcker, J. Long-Term Memory Recursive Least Squares Online Identification of Highly Utilized Permanent Magnet Synchronous Motors for Finite-Control-Set Model Predictive Control. *IEEE Transactions on Power Electronics* **2023**, *38*, 1451-1467, doi:10.1109/TPEL.2022.3206598.
46. Liu, S.; Wang, Q.; Wang, G.; Li, B.; Ding, D.; Zhang, G.; Xu, D. Virtual-Axis Injection Based Online Parameter Identification of PMSM Considering Cross Coupling and Saturation Effects. *IEEE Transactions on Power Electronics* **2023**, *38*, 5791-5802, doi:10.1109/TPEL.2023.3236031.

47. Sun, X.; Zhang, Y.; Lei, G.; Guo, Y.; Zhu, J. An Improved Deadbeat Predictive Stator Flux Control With Reduced-Order Disturbance Observer for In-Wheel PMSMs. *IEEE/ASME Transactions on Mechatronics* **2022**, *27*, 690-700, doi:10.1109/TMECH.2021.3068973.
48. Mwasilu, F.; Nguyen, H.T.; Choi, H.H.; Jung, J. Finite Set Model Predictive Control of Interior PM Synchronous Motor Drives With an External Disturbance Rejection Technique. *IEEE/ASME Transactions on Mechatronics* **2017**, *22*, 762-773, doi:10.1109/TMECH.2016.2632859.
49. Li, T.; Sun, X.; Yao, M.; Guo, D.; Sun, Y. Improved Finite Control Set Model Predictive Current Control for Permanent Magnet Synchronous Motor with Sliding Mode Observer. *IEEE Transactions on Transportation Electrification* **2023**, 10.1109/TTE.2023.3293510, 1-1, doi:10.1109/TTE.2023.3293510.
50. Li, L.; Liu, Y.; Li, Z.-H. Parameters Sensitivity Analysis of Predictive Current Control of Permanent Magnet Synchronous Motor Based on Extended State Observer. In Proceedings of 2020 5th International Conference on Electromechanical Control Technology and Transportation (ICECTT); pp. 321-325.
51. Sun, X.; Cao, J.; Lei, G.; Guo, Y.; Zhu, J. A Robust Deadbeat Predictive Controller With Delay Compensation Based on Composite Sliding-Mode Observer for PMSMs. *IEEE Transactions on Power Electronics* **2021**, *36*, 10742-10752, doi:10.1109/TPEL.2021.3063226.
52. Zhang, X.; Hou, B.; Mei, Y. Deadbeat Predictive Current Control of Permanent-Magnet Synchronous Motors with Stator Current and Disturbance Observer. *IEEE Transactions on Power Electronics* **2017**, *32*, 3818-3834, doi:10.1109/TPEL.2016.2592534.
53. Jiang, X.; Yang, Y.; Fan, M.; Ji, A.; Xiao, Y.; Zhang, X.; Zhang, W.; Garcia, C.; Vazquez, S.; Rodriguez, J. An Improved Implicit Model Predictive Current Control With Continuous Control Set for PMSM Drives. *IEEE Transactions on Transportation Electrification* **2022**, *8*, 2444-2455, doi:10.1109/TTE.2022.3144667.